Geophysical Journal International

Geophys. J. Int. (2017) **210,** 420–427
Advance Access publication 2017 April 26
GJI Geodynamics and tectonics

doi: 10.1093/gji/ggx171

Slip distribution of the 2015 Lefkada earthquake and its implications for fault segmentation

Lidong Bie,[1] Pablo J. González[2,*] and Andreas Rietbrock[1]

[1]*Liverpool Earth Observatory, School of Environmental Sciences, University of Liverpool, Liverpool, United Kingdom. E-mail: l.bie@liv.ac.uk*
[2]*COMET and Institute of Geophysics and Tectonics, University of Leeds, Leeds, United Kingdom*

Accepted 2017 April 25. Received 2017 April 24; in original form 2016 September 5

SUMMARY

It is widely accepted that fault segmentation limits earthquake rupture propagations and therefore earthquake size. While along-strike segmentation of continental strike-slip faults is well observed, direct evidence for segmentation of off-shore strike-slip faults is rare. A comparison of rupture behaviours in multiple earthquakes might help reveal the characteristics of fault segmentation. In this work, we study the 2015 Lefkada earthquake, which ruptured a major active strike slip fault offshore Lefkada Island, Greece. We report ground deformation mainly on the Lefkada Island measured by interferometric synthetic radar (InSAR), and infer a coseismic distributed slip model. To investigate how the fault location affects the inferred displacement based on our InSAR observations, we conduct a suite of inversions by taking various fault location from different studies as *a prior*. The result of these test inversions suggests that the Lefkada fault trace is located just offshore Lefkada Island. Our preferred model shows that the 2015 earthquake main slip patches are confined to shallow depth (<10 km), with a maximum slip of ∼1.6 m. In comparison to the 2003 earthquake, which mainly ruptured the northern part of the Lefkada fault, we suggest that the 2015 earthquake closed the seismic gap, at least partially, left by the 2003 earthquake by rupturing the shallow part of the Lefkada fault. The spatial variation in slip distributions for the two earthquakes reveals segmentation along strike, and possibly downdip of the Lefkada fault. A comparison of aftershock locations and coseismic slip distribution shows that most aftershocks appear near the edge of main coseismic slip patches.

Key words: Radar interferometry; Europe; Earthquake source observations.

1 INTRODUCTION

On 2015 November 17, a magnitude 6.5 earthquake struck Lefkada Island, Greece (Fig. 1). The NNE–SSW alignment of aftershocks following this earthquake suggests rupture of the Cephalonia-Lefkada Transform fault (CTF), a major tectonic structure in the Ionian area. The CTF comprises two segments, ∼40 km long Lefkada fault in the north near the coast of Lefkada Island, and ∼90 km long Cephalonia fault in the south with a slightly eastward tilting strike (Louvari *et al.* 1999; Kokinou *et al.* 2006). The northeastern end of CTF is marked by continental collision between NW Greece and the Apulian platform, while in the southwest lies the Hellenic subduction zone (e.g. Le Pichon *et al.* 1995; Papazachos & Kiratzi 1996). The CTF accommodates thrust motion at its two ends by a right-lateral slip motion at a rate of 2–3 cm yr^{-1} (e.g. Lagios *et al.* 2007; Pérouse *et al.* 2012; Ganas *et al.* 2013; Vernant *et al.* 2014). Briole *et al.* (2015) found an interseismic slip rate of 1.85–1.95 cm yr^{-1} for the southern Cephalonia segment, which is at the lower end of the above range of slip rate.

In a recent seismic zonation model for shallow earthquakes in the Aegean area (Vamvakaris *et al.* 2016), the islands of Lefkada, Cephalonia and Zakynthos are estimated to suffer shallow earthquakes of magnitude greater than 6.6 approximately every 50 yr. Short return-period of $M > 6$ earthquakes and high level of seismicity make this area one of the most seismically active in the eastern Mediterranean region (Papazachos 1996). For the Lefkada fault, it has been documented at least nine strong earthquakes with magnitude greater than 6 in the last 300 yr (Papazachos & Papazachou 2002). The majority of these destructive earthquakes occurred close to the northwestern part of the Lefkada Island, while the southwest edge has experienced fewer (Papazachos & Papazachou 2002). Only two earthquakes with magnitude 6.7 and 6.5 possibly occurred in the southwestern part in 1723 and 1948, respectively (Papadimitriou *et al.* 2006). The most recent earthquake that ruptured the Lefkada

* Now at: COMET and Liverpool Earth Observatory, School of Environmental Sciences, University of Liverpool, Liverpool, United Kingdom.

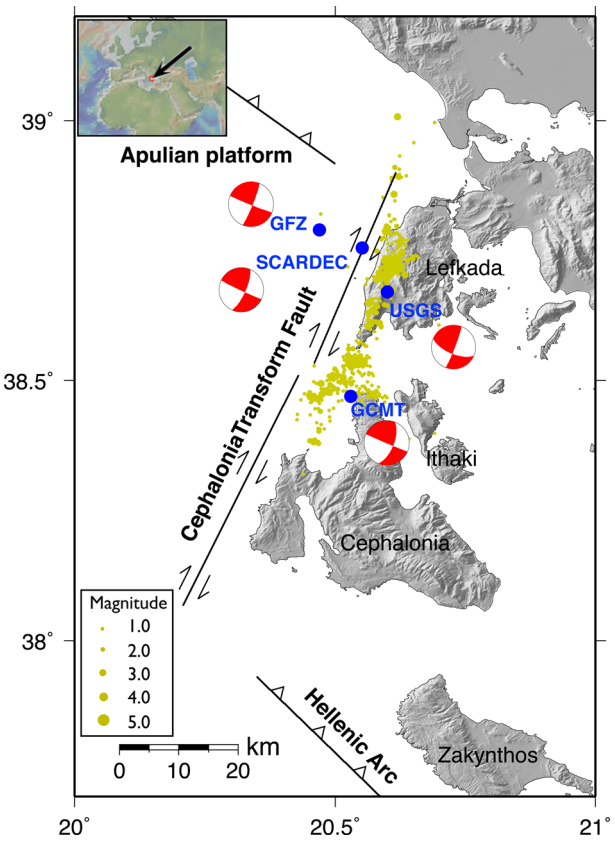

Figure 1. Seismotectonic setting of the Ionian Sea region. Fault traces are from Papadimitriou *et al*. (2006). Yellow points represent relocated aftershocks until 2015 December of 30 with local magnitude greater than 1 from the catalogue of National Observatory of Athens (Ganas *et al.* 2016). Earthquake location of the 2015 earthquake is marked as blue points, with corresponding publishing institution and focal mechanism solution labelled.

fault occurred on 2003 August 14 with magnitude 6.2. Based on seismic waveform modelling, Benetatos *et al*. (2007) found that the 2003 earthquake occurred as two subevents, separated by approximately 40 km in space, and slip was mainly deeper than 10 km. Ilieva *et al*. (2016), based on InSAR observations, reported a different rupture area for the 2003 event locating the main slip area in the northern part of the Lefkada fault. The remaining seismic gap on the Lefkada fault after the 2003 event was filled later by the recent 2015 earthquake (Chousianitis *et al.* 2016; Ganas *et al.* 2016; Sokos *et al.* 2016).

Several estimates locate the 2015 M_w 6.5 earthquake hypocentre along the southern part of the Lefkada Island, in respect to the 2003 earthquake. Focal mechanism solutions from different institutes are consistent in suggesting major right-lateral slip with minor dip-slip component on a steep SE-dipping fault (Fig. 1). Sokos *et al*. (2016) proposed that the 2015 earthquake consists of at least two subevents with right-lateral slip, and a third less reliable subevent with normal faulting slip. They also proposed that the Lefkada fault has its surface trace on the Lefkada Island. Distributed slip presented by Sokos *et al*. (2016) agrees well with the results from joint inversion of seismic and GPS observations (Chousianitis *et al*. 2016), showing two major slip patches at shallow depth, and unilateral rupture propagation to SSW of the Lefkada fault. Additionally, Ganas *et al*. (2016) presented uniform slip on a rectangular right-lateral fault plane from geodetic observations. An additional small fault rupture with reverse slip component was included by the authors to accommodate the displacement pattern shown by InSAR data. It would be interesting to see whether a single distributed slip model can reconcile the InSAR observations.

In this study, we report ground deformation observed by InSAR, invert for coseismic slip distribution from InSAR observations, and compare the amount of slip released with that has been accumulated since the last event in 1948. The abundant number of recorded aftershocks allows us to further investigate how aftershocks relate spatially with the coseismic slip distribution. Most importantly, the two earthquakes in 2003 and 2015 offer a chance to infer the partitioning of fault rupture and reveal fault segmentation characteristics on the Lefkada fault by comparing the two slip distributions.

2 InSAR DATA AND PROCESSING

Ground deformation associated with the Lefkada earthquake was obtained from InSAR observations. The InSAR data consist of ascending and descending Sentinel-1A data (Table 1) provided by the European Space Agency (ESA) with a wavelength of ∼5.55 cm. Both interferograms cover a period of 12 days. Sentinel-1 single-look complex (SLC) data were downloaded directly from the ESA scientific data hub. Interferograms were obtained using GAMMA@ following the procedure outlined in González *et al*. (2015). Shuttle Radar Topography Mission (SRTM) digital elevation model (Farr *et al.* 2007) was employed to remove the topographic contribution in the phase. Atmospheric noise was simulated and removed using ERA-Interim data (Jolivet *et al.* 2011; Walters *et al.* 2013). The interferograms were recursively filtered (González 2015), unwrapped using a minimum cost flow algorithm (Chen & Zebker 2000) and finally geocoded.

The interferograms show coseismic displacements on the southwestern part of Lefkada Island (Figs 2a and e). Both ascending and descending tracks reveal minor displacements on the northern tip of Cephalonia Island, indicating that the coseismic fault slip might have propagated as south as to Cephalonia Island. Line-of-sight (LOS) displacement revealed by the ascending data shows motion towards the satellite on both Lefkada and Cephalonia Islands, while displacement shown by the descending data is more complicated. In the descending data, a small area with negative LOS displacement in south Lefkada Island was surrounded by a large area of positive displacement (Fig. 2e). The difference in LOS displacement pattern results from different satellite viewing geometries. Given the fact that the descending track is mainly sensitive to vertical displacements, the area showing negative LOS displacements indicate a component of motion in the dip direction of the fault. Indeed, to reproduce this observation, Ganas *et al*. (2016) included an additional fault patch showing oblique slip of 0.6 m in both right lateral and reverse components. In the next section, we conduct a series of inversions to identify an optimal set of source parameters and distributed slip that can better fit the InSAR observations.

Table 1. SAR data used in this study.

Flight direction	Track	Master (YYYY/MM/DD)	Slave (YYYY/MM/DD)	Perpendicular Baseline (m)	Time difference
Ascending	175	2015 11 05	2015 11 17	25.8	12
Descending	80	2015 11 11	2015 11 23	66.2	12

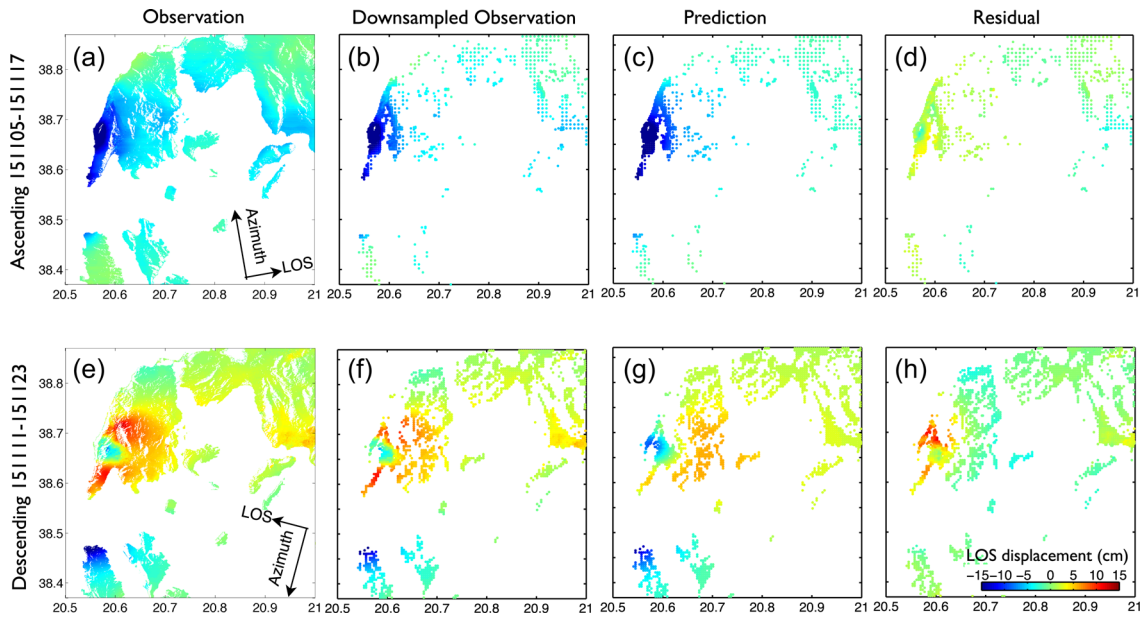

Figure 2. The observed, downsampled and modelled unwrapped coseismic InSAR data for ascending (upper row) and descending (bottom row) tracks. Details of the original interferograms are listed in Table 1. The modelled InSAR coseismic displacements (third column) were produced using our preferred distributed slip model, as shown in Fig. 3 and explained in Section 3.2.3. Here, positive displacement corresponds to a movement away from the satellite.

3 SLIP MODEL

Determining source parameters for earthquakes from InSAR observations is becoming increasingly routine, especially with a growing observing capacity of satellites in orbit (Weston *et al.* 2012). In Section 3.1, we follow the common procedure to estimate first an optimal set of source parameters including fault location, strike, dip, rake, size of the fault, and uniform slip. In Section 3.2, we invert for distributed slip by fixing the fault geometry. Given the fact that the epicentral area of the Lefkada earthquake is not fully imaged (the whole western side of the fault was incoherent due to water coverage), the fault location obtained from the uniform slip inversion may be less well constrained and could result in a biased distributed slip. This leads us to conduct three tests using different fault locations given by uniform slip inversion (this study), multi-source moment tensor inversion (Sokos *et al.* 2016) and previous studies (e.g. Benetatos *et al.* 2007). The three fault locations (Supporting Information Fig. S1) are numbered in order with our tests described in Section 3.2.

In accordance with the slip inversion of seismic data (Sokos *et al.* 2016), we also adopt the 1-D seismic velocity structure of the Ionian region proposed by Haslinger *et al.* (1999) for all our inversions. Both tracks of InSAR data were downsampled from millions to thousands of pixels (Figs 2b and f) to reduce computation cost, using the quadtree decomposition algorithm (Jónsson *et al.* 2002). A full variance-covariance matrix was then constructed for the downsampled data sets and used to generate the weighting matrix and synthetic spatially correlated noise (e.g. Cervelli *et al.* 2001; Bie *et al.* 2014).

3.1 Uniform slip model

To determine the fault orientation and source parameters for the 2015 Lefkada earthquake, we conduct a joint inversion of downsampled descending and ascending interferograms. The uniform slip inversion methodology is the same as used in Bie *et al.* (2014), where the Green's functions due to unitary slip in a layered Elastic earth were computed by the EDGRN/EDCMP package (Wang *et al.* 2003).

To seek optimal source parameters, we follow the routine procedure to simulate ground deformation using nonlinear optimization to search various combinations of those parameters within certain range (e.g. Cervelli *et al.* 2001; Bie *et al.* 2014). This methodology employed a simulated annealing algorithm and downhill simplex method to find the optimal parameters that minimize the weighted root-mean-square of residuals. In order to determine the errors of source parameters, we first create 100 sets of noise-perturbed data sets by adding the synthetic noise to the downsampled interferograms. Then, each data set is inverted independently using the nonlinear optimization to obtain a set of best fitting source parameters. The trade-off plot of 100 sets of source parameters (Supporting Information Fig. S2) shows an optimal fault striking N21°E and dipping 73° towards the east-southeast, with a dextral slip sense combined with a minor thrust component. The result obtained here (Supporting Information Table S1) is consistent with the focal mechanism reported by Papadimitriou *et al.* (2015), of which the strike/dip/rake values are 22°/72°/161°. Ganas *et al.* (2016) reported 18°/71°/180° for strike/dip/rake from inversion of geodetic observations for a uniform slip model, which is also similar to our results. The error associated with the fault location from our uniform slip modelling is ∼7 km in longitudinal direction, and ∼6 km in the latitudinal direction. We further explore in Section 3.2 how the fault location affects distributed slip modelling.

3.2 Distributed slip model

3.2.1 Test 1—fault location from our uniform slip modelling

In this test, we perform a weighted least-squares inversion for distributed slip on an extended fault plane (60 km in length by 30 km in width). We fix fault location (marked No. 1 in Supporting Information Fig. S1), strike and dip as obtained from the uniform slip modelling (Section 3.1). The distributed slip model comprises

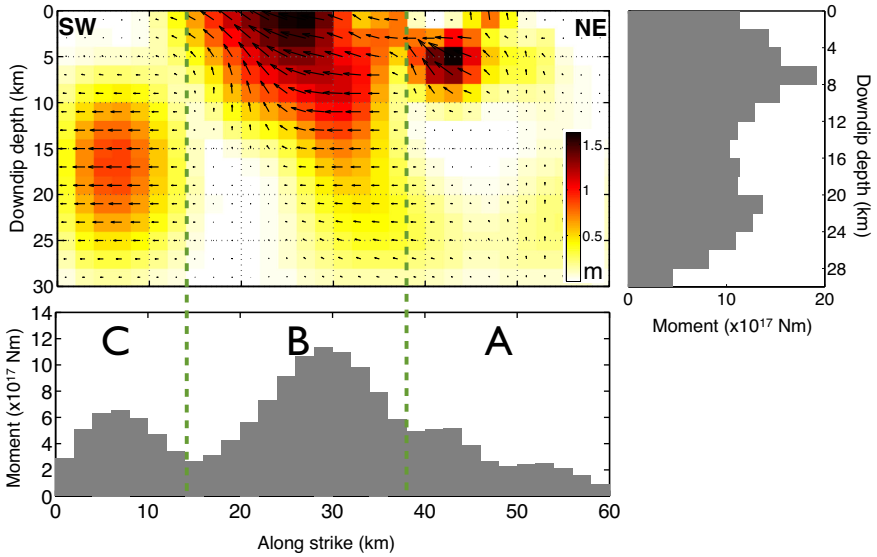

Figure 3. Preferred coseismic slip distribution model for the Lefkada earthquake (corresponding to Test 3 in Section 3.2) inverted from InSAR observations. Histogram plots show moment releases along the striking and in the downdip direction of the fault.

three slip patches, with the major one in the middle (Supporting Information Fig. S3a). Predicted LOS deformation is larger than observation for ascending track, while the prediction of descending track fails to reproduce the pattern of displacement observed on Lefkada Island (Supporting Information Fig. S4). This disagreement leads us to further investigate whether the location of the fault might play a role in fitting the data, given the large error bound of fault location. Next, we test a fault location from multi-source moment tensor inversion by Sokos *et al*. (2016), who suggested a fault having its surface extension right on Lefkada Island.

3.2.2 Test 2—fault location from multi-source moment tensor inversion

In the second test, we construct a fault plane passing through the earthquake centroids provided by Sokos *et al.* (2016). The fault (marked No. 2 in Supporting Information Fig. S1) locates approximately ∼20 km to the south and ∼10 km to the east of the fault (marked No. 1 in Supporting Information Fig. S1) estimated from the inversion of the InSAR measurements. Although the derived distributed slip model also has three slip patches (Supporting Information Fig. S3b), the predicted displacements and observations show no consistency (Supporting Information Fig. S5). The inconsistency suggests that the fault deduced from moment tensor inversion (Sokos *et al.* 2016) does not satisfy InSAR observations.

3.2.3 Test 3—fault location from previous studies

In a third test, we took the fault trace proposed by Papadimitriou *et al*. (2006) for the 2003 M_w 6.2 earthquake as *a priori* to construct the rupture plane. In fact, Benetatos *et al*. (2007) also used this fault location to recover the slip distribution for the 2003 earthquake using seismic observations. The slip distribution we obtained was again composed by three patches (Fig. 3), spatially consistent with that obtained by joint seismic and geodetic study (Chousianitis *et al.* 2016). In comparison to previous tests (Supporting Information Figs S4 and S5), the misfit between predicted and observed LOS displacement is greatly reduced for the ascending track (Fig. 2). The LOS displacement field shown by the descending data on Lefkada Island is also recovered (Figs 2f and g), although the local residual signal near the coast persist (Fig. 2h). The residuals of our coseismic slip model might be due to complexities in the coseismic rupture or early post-seismic phase in this region. We also note that, the positive residual near the coast in Fig. 2(h) corresponds to where Papathanassiou *et al.* (2017) found extensive earthquake-induced failure, such as landslide. In the following analysis, we take the distributed slip model in the third test as our preferred model (Fig. 3), since it gives the best overall fit to the observed deformation.

The observed slip distribution has three peaks (Fig. 3). Slip patch A locates above the hypocentre, confined to the upper 10 km, indicating an initial up-dip propagation of rupture. Then, the rupture propagates unilaterally towards SSW, leading to the main moment release on patch B, off the south-western coast of Lefkada Island. Slip patch B is confined to an area with length of ∼25 km, extending from surface and smearing to 25 km in depth. The maximum slip is ∼1.6 m, nearly five times larger than that of the 2003 earthquake (Benetatos *et al.* 2007). Slip on patches A and B comprises thrusting and shearing components. Slip patch C shows a pure dextral slip, with maximum slip reaching 0.9 m.

Furthermore, we perform resolution tests (Fig. 4) to assess how well the features in our distributed slip model are resolved. It is clearly shown in Fig. 4 that the slip is less-well resolved in amplitude and location at depth greater than 10 km. In the along-strike direction of the fault, slip on the NE part of the fault plane is better resolved than the SW part, partially due to the fault closeness to the island where the displacements are densely imaged. In comparison to the distributed slip model from Chousianitis *et al*. (2016), which was constrained by seismic and GPS data, our model shows agreement in the location of two major slip patches A and B. As to the slip patch C, given that it locates in a poorly resolved area (SW of the fault and deeper than 10 km), we are less confident in its robustness. We run a test to investigate how removing slip on patch C affects recovering of InSAR observations (Supporting Information Fig. S6). The performed test shows that the ascending data does not necessarily require slip on this part of the fault. However, the patch

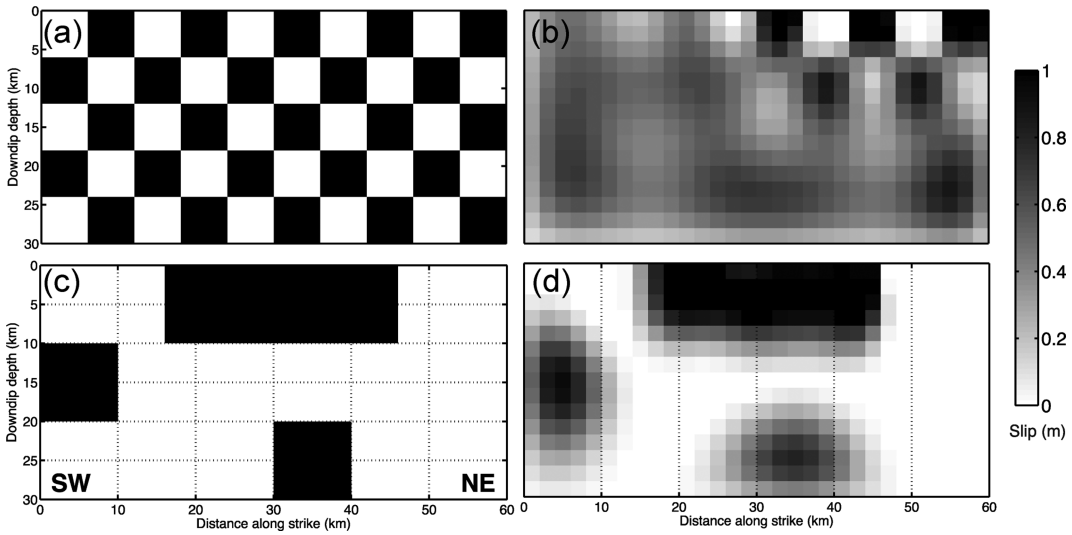

Figure 4. Checkerboard test showing the spatial resolution of distributed slip inversion from InSAR: left-hand (a,c) panels showing the input slip model and right-hand panels (b,d) showing the recovered slip distribution. The resolution tests show that the slip is less-well resolved at depth greater than 10 km. In the along-strike direction of the fault, slip on the NE part of the fault plane is better resolved than the SW part.

C is needed to satisfy the deformation imaged on the northern tip of Cephalonia Island observed by the descending data (Supporting Information Fig. S6).

4 DISCUSSION

4.1 InSAR constraints on slip model of offshore earthquakes

InSAR has been greatly successful in determining earthquake source parameters. For shallow earthquakes, Weston *et al*. (2012) found that InSAR-derived source locations are more accurate than those derived by seismic data. By using InSAR observations, Lohman & Simons (2005) precisely located four small earthquakes in the Zagros Mountains that would otherwise be too small to be well-located. One reason of its success in precise determination of earthquake location is that InSAR can provide dense observations over epicentral area. Typically, a strike-slip earthquake causes a four-quadrant displacement field. It is therefore fairly straightforward to determine accurately fault location as in between the quadrants where the sign of displacement changes. With multiple observations from various satellites, 3-D displacements can still be obtained, providing additional constraints on the fault trace (e.g. Wright *et al.* 2004). Unlike continental strike-slip earthquakes, where InSAR is capable of providing full coverage of deformed area, offshore earthquakes induce ground deformation that can only be partially observed on nearby land areas.

The ground deformation mapped for the Lefkada earthquake challenges the traditional inversion strategy for distributed slip along continental strike-slip faults as demonstrated in Section 3.2. With the whole western side of the Lefkada fault lacking InSAR observations, the fault location obtained from uniform slip modelling is less well constrained. The potential uncertainty in fault location could further affect the next step of inversion for distributed slip, for which the fault location is often fixed as a known parameter similar to distributed slip inversions along the subduction zone megathrust.

It is a common practice that certain source parameters are taken as *a priori* in InSAR inversions. For example, when a fault is well-mapped by other methods (e.g. geological mapping, seismic imaging, pixel offsets), the fault location can be treated as a known parameter in inversion for distributed slip (e.g. Bie & Ryder 2014). Geodetic studies of megathrust earthquakes often invert for distributed slip on an *a priori* interplate slab model, such as the 2011 Tohoku Oki earthquake (e.g. Simons *et al.* 2011) and 2010 Maule earthquake (e.g. Lin *et al.* 2013). In our second test (Section 3.2.2), although we used the fault location suggested by the seismic study, the fit to InSAR data is not satisfying. It is worthy to note that our preferred fault (test 3 in Section 3.2.3) locates in between the faults derived independently from InSAR and seismic studies (Supporting Information Fig. S1). This implies that a joint inversion of both data sets may be helpful in resolving more accurately fault location of similar tectonic settings and will be discussed in a future study.

4.2 Coseismic slip and aftershocks

One interesting topic in earthquake science is the spatial relationship between aftershocks and distributed coseismic slip, which may have implications to understanding heterogeneities in fault properties (barriers or asperities). Previous studies on aftershock distribution following strike-slip earthquakes tend to find that aftershocks occur mostly outside of or near the edges of the coseismic slip (e.g. Mendoza & Hartzell 1988; Rietbrock *et al*. 2012).

Fig. 5 shows the surface projection of spatial relationship between coseismic slip and aftershocks. Here, 960 aftershocks were relocated by Ganas *et al.* (2016) from the catalogue provided by National Observatory of Athens (NOA) between 2015 November 17 and December 30. The relocation used only arrivals from stations within 120 km of the main shock and the errors in horizontal and depth directions are smaller than 3 km (Ganas *et al.* 2016). We project aftershocks within 10 km either side of the main-shock fault plane onto the fault. It is apparent that aftershocks following the 2015 earthquakes mostly appear near the edge of coseismic slip patches. A large cluster of aftershocks is found SW below the main

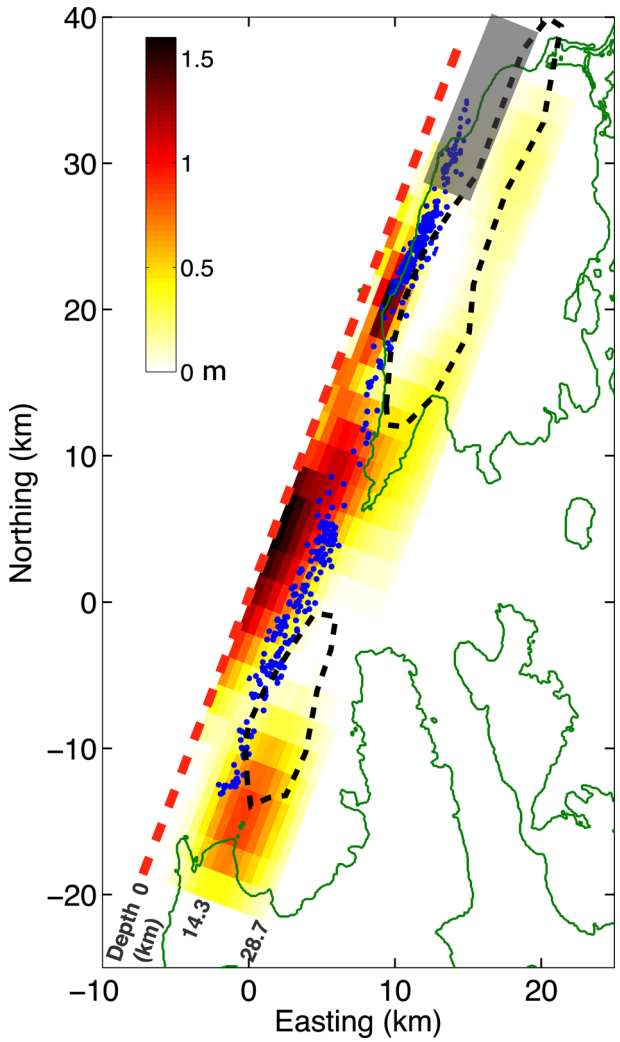

Figure 5. Spatial relationship between coseismic slip distribution and aftershocks of the 2015 earthquake. Black dashed lines depict the coseismic rupture as proposed by Benetatos *et al*. (2007), and grey rectangular area shows the uniform slip area estimated by Ilieva *et al*. (2016) for the 2003 earthquake. Aftershocks within 10 km from either side of the rupture are first projected onto the fault plane and then projected together with the rupture onto the surface. Green lines mark the coastline. Red thick dashed line indicates the surface rupture of the 2015 earthquake, being just offshore the Lefkada Island.

slip patch B. Similar to the 2015 Lefkada event, the 2003 M_w 6.6 Bam earthquake, another dextral slip event, also has most of its aftershocks near the bottom edge of the main coseismic slip (Tatar *et al.* 2005). On the contrary, aftershocks in first week following the 2003 earthquake appear above the coseismic slip patches (see fig. 6 of Benetatos *et al.* 2007). One interesting question is whether the aftershocks following 2003 and 2015 earthquakes are in the same region. If so, this region might represent a persistent barrier that stops rupture propagation up- or downdip on this part of the fault and thus separates two asperities above and below it, causing a segmental behaviour in this direction. However, regarding the inference of segmental behaviour in down-dip direction, we realize that it partly depends on the spatial comparison between distributed slip models for the 2003 and 2015 earthquakes, which we explore more in Section 4.3.

4.3 Fault segmentation and seismic gap

Fault segmentation has critical implications for the dynamics and size of earthquake ruptures (De Joussineau & Aydin 2009). It has been long recognized that, for strike-slip faults, segment boundaries such as fault steps might impede or arrest the propagation of seismic rupture (e.g. Wesnousky 2006), thus limiting the earthquake size and potential damage. For a seismically active region, such as the Ionian area, it is critically important to understand the fault characteristics in terms of segmentation, which affects the estimation of potential maximum earthquake magnitude. By comparing the slip models of two recent earthquakes on the Lefkada fault, we therefore may gain some insights into the possible fault segmentation.

As shown by our modelling results, the 2015 earthquake ruptured generally the shallow part of the Lefkada fault (<10 km), although the main slip patch (patch B in Fig. 3) smears to ∼25 km depth. This feature of shallow slip is consistent with the distributed slip model suggested by Chousianitis *et al*. (2016). In the contrary, as introduced in the Section 1, there is currently no consensus on the slip model for the 2003 earthquake. Two independent slip inversion studies based on various data sets exist. From inversion of seismic data, Benetatos *et al*. (2007) obtained a slip model with two major patches on the deeper part of Lefkada fault (between depths of 10–25 km) for the 2003 event. Based on the larger depth they found for the 2003 earthquake, they propose a thicker brittle crust for this region. Modelling of InSAR data for the 2003 earthquake, however, indicated rupture mainly on the northern part of the Lefkada fault (see fig. 1 of Ilieva *et al*. 2016) at shallow depth. The SW end from the uniform slip model of the 2003 earthquake is adjacent to slip patch A of our distributed slip model for the 2015 earthquake (Fig. 5).

A likely explanation to the difference of slip models for the 2003 earthquake is, they used a different fault geometry to retrieve slip. Benetatos *et al*. (2007) fixed the dip of Lefkada fault at 81°, much larger than 59°, which was adopted by Ilieva *et al*. (2016) from Harvard CMT solution. The large difference in fault steepness can introduced significant variation of inferred slip depth. The depth of slip obtained using a dip angle of 81° could be as 3.8 times larger as that derived from using 59° (Supporting Information Fig. S7), assuming the same fault surface trace and other source parameters. This explains an upper edge of 3.5 km reported by Ilieva *et al*. (2016) in the uniform slip model and an upper edge of ∼10 km from Benetatos *et al*. (2007) in their distributed slip model for the 2003 earthquake. Regardless of the disagreement in slip models of the 2003 earthquake, it is obvious from Fig. 5 that the 2015 earthquake ruptured a different area on the Lefkada fault, indicating fault segmentation at least along strike of the fault. Whether downdip segmentation of the Lefkada fault exits remains an open question to answer. A joint inversion of seismic and geodetic data or separate inversions with consistent *a priori* constraints would be needed to refine the distributed slip model for the 2003 earthquake, and in turn, may help answer whether there exists segmentation downdip the Lefkada fault.

Considering an interseismic slip rate of 2–3 cm yr^{-1} (e.g. Ganas *et al.* 2013; Vernant *et al.* 2014) and assuming all strain is accumulated along a fully locked Lefkada fault system, a segment corresponding to 2015 earthquake slip patch B (Fig. 3) has accumulated between 1.34 and 2.01 m of slip deficit since the last major event in 1948. With a maximum slip of ∼1.6 m, the 2015 earthquake closed, at least partially, the seismic gap left by the 2003 M_w 6.2 earthquake on the Lefkada fault.

5 CONCLUSIONS

This work presents Sentinel-1 InSAR observations of the coseismic displacement associated with the 2015 M_w 6.5 Lefkada earthquake, Greece. Given the fact that the earthquake ruptured an offshore strike-slip fault, InSAR only recorded partially the coseismic displacements, leading to a less well-constrained fault location and slip distribution based on uniform slip inversion result from InSAR data alone. Additionally, we tested the inversion procedure by taking the fault location inferred from seismic study of moment tensor as *a priori* and found that the predicted ground deformation does not match the InSAR observations. This disagreement tends to put the favoured fault location in between those derived by geodetic or seismic data separately. Our preferred slip model, together with resolution tests, show that major slip of the 2015 earthquake is confined to shallow depths (<10 km). Although there are competing models for the slip distribution of the 2003 earthquake locating the upper edge of main slip patch at shallower (3.5 km) or larger (10 km) depth, it is clear that the 2015 earthquake ruptured a different area in comparison to the 2003 events, indicating segmentation along strike of the Lefkada fault. The 2015 earthquake closed the seismic gap, at least partially, left by the 2003 earthquake by rupturing mainly the shallow part of the Lefkada fault. Finally, a comparison of aftershock and coseismic slip distribution shows that most aftershocks appear near the edge of main coseismic slip patches.

ACKNOWLEDGEMENTS

We thank the editor (Prof Duncan Agnew) and two anonymous reviewers for their helpful comments. This work was partially supported by the UK Natural Environmental Research Council (NERC) through NE/K011006/1, NE/P008828/1, and the Centre for the Observation and Modelling of Earthquakes, Volcanoes and Tectonics (COMET, GA/13/M/031, http://comet.nerc.ac.uk). The Sentinel-1 interferograms presented are a derived work of Copernicus data, subject to the ESA use and distribution conditions. We thank Dr Stephen Hicks for constructive comments on an early version of this paper.

REFERENCES

Benetatos, C., Dreger, D. & Kiratzi, A., 2007. Complex and segmented rupture associated with the 14 August 2003 M_w 6.2 Lefkada, Ionian Islands, earthquake, *Bull. seism. Soc. Am.,* **97**(1B), 35–51.

Bie, L. & Ryder, I., 2014. Recent seismic and aseismic activity in the Ashikule stepover zone, NW Tibet, *Geophys. J. Int.,* **198**(3), 1632–1643.

Bie, L., Ryder, I., Nippress, S.E. & Bürgmann, R., 2014. Coseismic and postseismic activity associated with the 2008 M_w 6.3 Damxung earthquake, Tibet, constrained by InSAR, *Geophys. J. Int.,* **196**(2), 788–803.

Briole, P. *et al.*, 2015. The seismic sequence of January–February 2014 at Cephalonia Island (Greece): constraints from SAR interferometry and GPS, *Geophys. J. Int.,* **203**(3), 1528–1540.

Cervelli, P., Murray, M.H., Segall, P., Aoki, Y. & Kato, T., 2001. Estimating source parameters from deformation data, with an application to the March 1997 earthquake swarm off the Izu Peninsula, Japan, *J. geophys. Res.,* **106**(B6), 11 217–11 238.

Chen, C.W. & Zebker, H.A., 2000. Network approaches to two-dimensional phase unwrapping: intractability and two new algorithms, *J. Opt. Soc. Am.,* **17**(3), 401–414.

Chousianitis, K., Konca, A.O., Tselentis, G., Papadopoulos, G.A. & Gianniou, M., 2016. Slip model of the 17 November 2015 $M_w = 6.5$ Lefkada earthquake from the joint inversion of geodetic and seismic data, *Geophys. Res. Lett.,* **43**(15), 7973–7981.

De Joussineau, G. & Aydin, A., 2009. Segmentation along strike-slip faults revisited, in *Mechanics, Structure and Evolution of Fault Zones,* pp. 1575–1594, eds Ben-Zion, Y. & Sammis, C., Birkhäuser.

Farr, T.G. *et al.*, 2007. The Shuttle Radar Topography Mission, *Rev. Geophys.,* **45**(2), doi:10.1029/2005RG000183.

Ganas, A. *et al.*, 2016. Coseismic deformation, field observations and seismic fault of the 17 November 2015 $M = 6.5$, Lefkada Island, Greece earthquake, *Tectonophysics,* **687,** 210–222.

Ganas, A., Marinou, A., Anastasiou, D., Paradissis, D., Papazissi, K., Tzavaras, P. & Drakatos, G., 2013. GPS-derived estimates of crustal deformation in the central and north Ionian Sea, Greece: 3-yr results from NOANET continuous network data, *J. Geodyn*., **67,** 62–71.

González, P.J., 2015. RSF: a robust non-parametric phase filtering method for automatic processing of Sentinel-1 interferograms, in *FRINGE 2015 Workshop,* ESA.

González, P.J., Bagnardi, M., Hooper, A.J., Larsen, Y., Marinkovic, P., Samsonov, S.V. & Wright, T.J., 2015. The 2014–2015 eruption of Fogo volcano: Geodetic modeling of Sentinel-1 TOPS interferometry, *Geophys. Res. Lett.,* **42**(21), 9239–9246.

Haslinger, F. *et al.*, 1999. 3D crustal structure from local earthquake tomography around the Gulf of Arta (Ionian region, NW Greece), *Tectonophysics,* **304**(3), 201–218.

Ilieva, M., Briole, P., Ganas, A., Dimitrov, D., Elias, P., Mouratidis, A. & Charara, R., 2016. Fault plane modelling of the 2003 August 14 Lefkada Island (Greece) earthquake based on the analysis of ENVISAT SAR interferograms, *Tectonophysics,* **693,** 47–65.

Jolivet, R., Grandin, R., Lasserre, C., Doin, M.-P. & Peltzer, G., 2011. Systematic InSAR tropospheric phase delay corrections from global meteorological reanalysis data, *Geophys. Res. Lett.,* **38,** L17311, doi:10.1029/2011GL048757.

Jónsson, S., Zebker, H., Segall, P. & Amelung, F., 2002. Fault slip distribution of the 1999 M_w 7.1 Hector Mine, California, earthquake, estimated from satellite radar and GPS measurements, *Bull. seism. Soc. Am.,* **92**(4), 1377–1389.

Kokinou, E., Papadimitriou, E., Karakostas, V., Kamberis, E. & Vallianatos, F., 2006. The Kefalonia transform zone (offshore western Greece) with special emphasis to its prolongation towards the Ionian abyssal plain, *Mar. Geophys. Res*., **27**(4), 241–252.

Lagios, E., Sakkas, V., Papadimitriou, P., Parcharidis, I., Damiata, B.N., Chousianitis, K. & Vassilopoulou, S., 2007. Crustal deformation in the Central Ionian Islands (Greece): results from DGPS and DInSAR analyses (1995–2006), *Tectonophysics,* **444**(1), 119–145.

Le Pichon, X., Chamot-Rooke, N., Lallemant, S., Noomen, R. & Veis, G., 1995. Geodetic determination of the kinematics of central Greece with respect to Europe: implications for eastern Mediterranean tectonics, *J. geophys. Res.,* **100**(B7), 12 675–12 690.

Lin, Y.N.N. *et al.*, 2013. Coseismic and postseismic slip associated with the 2010 Maule Earthquake, Chile: characterizing the Arauco Peninsula barrier effect, *J. geophys. Res.,* **118**(6), 3142–3159.

Lohman, R.B. & Simons, M., 2005. Locations of selected small earthquakes in the Zagros mountains, *Geochem. Geophys. Geosyst.,* **6**(3), doi:10.1029/2004GC000849.

Louvari, E., Kiratzi, A.A. & Papazachos, B.C., 1999. The Cephalonia transform fault and its extension to western Lefkada Island (Greece), *Tectonophysics,* **308**(1), 223–236.

Mendoza, C. & Hartzell, S.H., 1988. Aftershock patterns and main shock faulting, *Bull. seism. Soc. Am.,* **78**(4), 1438–1449.

Papadimitriou, P., Kaviris, G. & Makropoulos, K., 2006. The $M_w = 6.3$ 2003 Lefkada earthquake (Greece) and induced stress transfer changes, *Tectonophysics,* **423**(1), 73–82.

Papadimitriou, P. *et al.*, 2015. 'Preliminary report on the Lefkada 17 November 2015 $M_w = 6.4$ earthquake'. Available at: http://www.emsc-csem.org/Doc/Additional_Earthquake_Report/470390/20151117_lefkada_report_nkua.pdf, last accessed February 2017.

Papathanassiou, G., Valkaniotis, S., Ganas, A., Grendas, N. & Kollia, E., 2017. The November 17th, 2015 Lefkada (Greece) strike-slip earthquake: field mapping of generated failures and assessment of macroseismic intensity ESI-07, *Eng. Geol.,* **220,** 13–30.

Papazachos, B.C., 1996. Large seismic faults in the Hellenic Arc, *Ann. Geofis.,* **39,** 891–903.
Papazachos, B.C. & Papazachou, C., 2002. *The Earthquakes of Greece,* Ziti Publ.
Papazachos, C.B. & Kiratzi, A.A., 1996. A detailed study of the active crustal deformation in the Aegean and surrounding area, *Tectonophysics,* **253**(1), 129–153.
Pérouse, E., Chamot-Rooke, N., Rabaute, A., Briole, P., Jouanne, F., Georgiev, I. & Dimitrov, D., 2012. Bridging onshore and offshore present-day kinematics of central and eastern Mediterranean: implications for crustal dynamics and mantle flow, *Geochem. Geophys. Geosyst.,* **13,** Q09013, doi:10.1029/2012GC004289.
Rietbrock, A., Ryder, I., Hayes, G., Haberland, C., Comte, D., Roecker, S. & Lyon-Caen, H., 2012. Aftershock seismicity of the 2010 Maule M_w = 8.8, Chile, earthquake: correlation between co-seismic slip models and aftershock distribution?, *Geophys. Res. Lett.,* **39,** L08310, doi:10.1029/2012GL051308.
Simons, M. *et al.*, 2011. The 2011 magnitude 9.0 Tohoku-Oki earthquake: Mosaicking the megathrust from seconds to centuries, *Science,* **332**(6036), 1421–1425.
Sokos, E., Zahradník, J., Gallovič, F., Serpetsidaki, A., Plicka, V. & Kiratzi, A., 2016. Asperity break after 12 years: the M_w6.4 2015 Lefkada (Greece) earthquake, *Geophys. Res. Lett.,* **43**(12), 6137–6145.
Tatar, M., Hatzfeld, D., Moradi, A.S. & Paul, A., 2005. The 2003 December 26 Bam earthquake (Iran), M_w 6.6, aftershock sequence, *Geophys. J. Int.,* **163**(1), 90–105.
Vamvakaris, D.A., Papazachos, C.B., Papaioannou, C.A., Scordilis, E.M. & Karakaisis, G.F., 2016. A detailed seismic zonation model for shallow earthquakes in the broader Aegean area, *Nat. Hazard Earth Syst. Sci.,* **16**(1), 55–84.
Vernant, P., Reilinger, R. & McClusky, S., 2014. Geodetic evidence for low coupling on the Hellenic subduction plate interface, *Earth planet. Sci. Lett.,* **385,** 122–129.
Walters, R.J., Elliott, J., Li, Z. & Parsons, B., 2013. Rapid strain accumulation on the Ashkabad fault (Turkmenistan) from atmosphere-corrected InSAR, *J. geophys. Res.,* **118,** 3674–3690.
Wang, R., Lorenzo Martin, F. & Roth, F., 2003. Comparison of deformation induced by earthquakes in a multi-layered elastic crust-FORTRAN programs EDGRN/EDCMP, *Comput. Geosci.,* **29,** 195–207.
Wesnousky, S.G., 2006. Predicting the endpoints of earthquake ruptures, *Nature,* **444**(7117), 358–360.
Weston, J., Ferreira, A.M. & Funning, G.J., 2012. Systematic comparisons of earthquake source models determined using InSAR and seismic data, *Tectonophysics,* **532,** 61–81.
Wright, T.J., Parsons, B.E. & Lu, Z., 2004. Toward mapping surface deformation in three dimensions using InSAR, *Geophys. Res. Lett.,* **31**(1), L01607, doi:10.1029/2003GL018827.

SUPPORTING INFORMATION

Supplementary data are available at *GJI* online.

Figure S1. 3-D map showing various *a priori* fault locations we tested. Each fault is labelled in sequence corresponding to the three tests in Section 3.2. Black thick lines show the surface extension of the three faults. Dashed line numbered 1 is the fault trace derived by our inversion of InSAR data for uniform slip. Fault trace marked 2 is constructed from multisource moment tensor inversion by Sokos *et al*. (2016). White solid line numbered 3 represents our preferred fault location. Red stars mark the centroid from multi-source moment tensor study by Sokos *et al*. (2016).

Figure S2. Trade-offs and uncertainties of source parameters for the Lefkada earthquake assuming uniform slip on a rectangular plane buried in a layered crust model. Red curves show Gaussian fit to the distribution of source parameters. Optimal values are also listed in Table S1.

Figure S3. Distributed slip models obtained from inversion of InSAR data. (a) Slip distribution from Test 1 with fault location fixed as obtained from our uniform slip inversion (parameters shown in Table S1). (b) Slip distribution from Test 2 with fault location fixed as obtained from multisource moment tensor inversion (Sokos *et al.* 2016). Fault locations can be found in Fig. S1.

Figure S4. Downsampled observation, prediction and residual for Test 1 (Section 3.2.1). It assumes a distributed slip model as shown in Fig. S3(a), which has its fault location fixed as obtained from uniform slip inversion in this study.

Figure S5. Downsampled observation, prediction and residual for Test 2 (Section 3.2.2). It assumes a distributed slip model as shown in Fig. S3(b). This slip model was obtained by fixing fault location as inferred from multi-source moment tensor inversion.

Figure S6. A test showing how removing slip on patch C in our preferred distributed slip model (shown in Fig. 3) affects recovering the downsampled InSAR observation. The only apparent difference from residuals shown in Fig. 2 is marked by a black circle in residual map for the descending track. It shows that slip patch C is only constrained by the descending data.

Figure S7. Schematic plot showing the likely trade-off of fault steepness and fault depth. Blue point marks surface displacement. Red and black lines correspond to the fault used by Benetatos *et al*. (2007) and Ilieva *et al*. (2016) in their inversion for slip model for the 2003 earthquake, respectively. A larger fixed fault dip (steeper) tends to favour a deeper-seated slip.

Table S1. Source parameters obtained from joint inversion of descending and ascending data, assuming a layered crust model.

Table S2. Downsampled ascending interferogram constructed by SAR acquisitions on 2015 November 1 and 17.

Table S3. Downsampled descending interferogram constructed by SAR acquisitions on 2015 November 11 and 23.

Table S4. Coseismic variable-slip model in a layered crust in Finite Source Parameter (FSP) format.

Please note: Oxford University Press is not responsible for the content or functionality of any supporting materials supplied by the authors. Any queries (other than missing material) should be directed to the corresponding author for the paper.